Femtosecond laser ablation of transparent microphotonic devices and computer-generated holograms

Alqurashi, Tawfiq; Montelongo, Yunuen; Penchev, Pavel; Yetisen, Ali K.; Dimov, Stefan; Butt, Haider

Document Version
Peer reviewed version

[Link to publication on Research at Birmingham portal](#)

Femtosecond Laser Ablation of Transparent Microphotonic Devices and Computer-Generated Holograms

*Tawfiq Alqurashi[a, b, *], Yunuen Montelongo[c], Pavel Penchev [a], Ali K. Yetisen[d], Stefan Dimov[a], and Haider Butt[a,*]*

[a]*School of Mechanical Engineering, University of Birmingham, Birmingham, B15 2TT, UK*

[b]*Department of Mechanical Engineering, School of Engineering, Shaqra University, Dawadmi, P.O. Box 90 Zip Code 11921, Saudi Arabia*

[c]*Department of Chemistry, Imperial College London, London, SW7 2AZ, UK*

[d]*Harvard-MIT Division of Health Sciences and Technology, Harvard University and Massachusetts Institute of Technology, Cambridge, MA, 02139, USA*

Abstract

Femtosecond laser ablation allows direct patterning of engineering materials in industrial settings without requiring multistage processes such as photolithography or electron beam lithography. However, femtosecond lasers have not been widely used to construct volumetric microphotonic devices and holograms with high reliability and cost efficiency. Here, a direct femtosecond laser writing process is developed to rapidly produce transmission 1D/2D gratings, Fresnel Zone Plate lenses, and computer-generated holograms. The optical properties including light transmission, angle-dependent resolution, and light polarization effects for the microphotonic devices have been characterized. Varying the depth of the microgratings from 400 nm to 1.5 µm allowed the control over their transmission intensity profile. The optical properties of the 1D/2D gratings were validated through a geometrical theory of diffraction model involving 2D phase modulation. The produced Fresnel lenses had transmission efficiency of ~60% at normal incidence and they preserved the polarization of incident light. The computer-generated holograms had an average transmission efficiency of 35% over the visible spectrum. These microphotonic devices had wettability resistance of contact angle ranging from 44° to 125°. These devices can be used in a variety of applications including wavelength-selective filters, dynamic displays, fiber optics, and biomedical devices.

Keywords: laser ablation, microphotonics, diffraction, Fresnel Zone Plate lens, holograms, gratings, phase modulation

Introduction

Femtosecond (FS) lasers have been widely used for the processing of polymers [1], metals [2, 3], and biological tissues [4]. Their applications also span across machining of submicrometer sized features on silica and silver substrates [5, 6], along with a myriad of large-area industrial applications [7-9]. The unique advantage of FS laser ablation of transparent materials is that they have a nonlinear nature of light absorption due to the lack of electronic transitions at the energy of the incident photon [10, 11]. This nonlinear absorption confines any induced change to the focal volume, allowing the fabrication of complex structures [12, 13]. Additionally, FS laser processing is a deterministic process [14, 15]. First, it has no thermal effect because the laser pulse ends before the electrons thermally excite any ion and the heat diffusion outside the focal area is minimized. This FS machining process reduces heating caused by expansion effects, leading to an increase in its patterning precision as compared to other laser patterning processes [16-18]. Hence, FS lasers have the potential to rapidly produce tailored and accurate nano- and microstructures in automated manufacturing systems [19, 20].

FS lasers have been utilized to pattern transparent materials for the fabrication of 1D gratings [21-24], 2D devices [25], and Fresnel zone plate (FZP) lenses [26, 27]. These approaches have utilized either amplified Ti:Sapphire systems or long-cavity oscillators, which have relatively lower powers and low pulse operating frequencies. Therefore, their fabrication speeds in patterning transparent materials are lower as compared to FS ytterbium-based laser sources, commonly used in optical device fabrication [28]. Here, the novelty was to integrate computer-generated holography (CGH) during laser fabrication process to predict its optical characteristics. Rapid direct FS laser writing of optical devices

3

through holographic patterning on transparent polycarbonate (PC) substrates has not been reported before. Hence, the development of a patterning approach employing highly dynamic FS laser sources can enable the cost-effective production of microphotonic devices on polymeric substrates.

Here, a FS ytterbium-based laser microstructuring method is demonstrated to produce microphotonic devices, 1/2D transmission gratings, Fresnel lenses and holograms in the visible spectrum range directly on a transparent PC substrate. PC has high light transmission efficiency, high-impact resistance, lightweight, and effective wettability resistance [29-31]. It has also been reported to have high thermal stability (thermo-optic coefficient of -1.06×10^{-4} °C^{-1} at 1550 nm), ease of processability, high adhesion, and low propagation losses in the visible spectrum (0.197 dB cm^{-1} at 632.8 nm) [32]. It is also well-known as a retardation film that produce high contrast and wide viewing-angle properties[33] and is needed for electroluminescence display to prevent the reflection of ambient light[34].The microphotonic devices were fabricated by using a FS ytterbium-based laser. This approach allowed patterning large areas of microstructures with a depth of few hundred nanometers to rapidly produce rigid and mechanically strong microphotonic devices and holograms as compared to other microfabrication techniques which require phase masks or photosensitive materials. In addition, a FS ytterbium-based laser has a higher fabrication speed as compared to other laser sources due to high pulse repetition frequency (2 MHz). Optical characteristics of the fabricated microphotonic structures with different depths were studied through periodic structure visualization; diffraction intensity profiling, angle-resolved measurements, and light output shape symmetry analysis. The groove depths can be used to control the phase modulation of light

Additionally, FFT has been utilized to write computer-generated holograms. Such microphotonic structures produce interference in the visible spectrum of light to create a desired light shape output. This fabrication approach combined with FFT simulations enables creating rationally-designed complex geometries that can produce any predicted shape, transmission intensity profile with precise diffraction angle, and the geometry of output. These microphotonic devices can be used in a wide variety of industrial applications including laser patterning, dynamic displays, sensors, fiber optics, and photomedicine [35].

FFT-based Design and Fabrication of Microphotonic Devices

The first step in the FS laser fabrication of the microphotonic devices was to rationally design microstructures using computational modelling (Figure 1a-c). A 1/2D transmission gratings, a Fresnel Zone Plate (FZP) lens and a hologram pattern were designed to provide predefined photonic characteristics. These designs were micropatterned using a FS laser on a large surface area of 2 mm thick PC substrates.
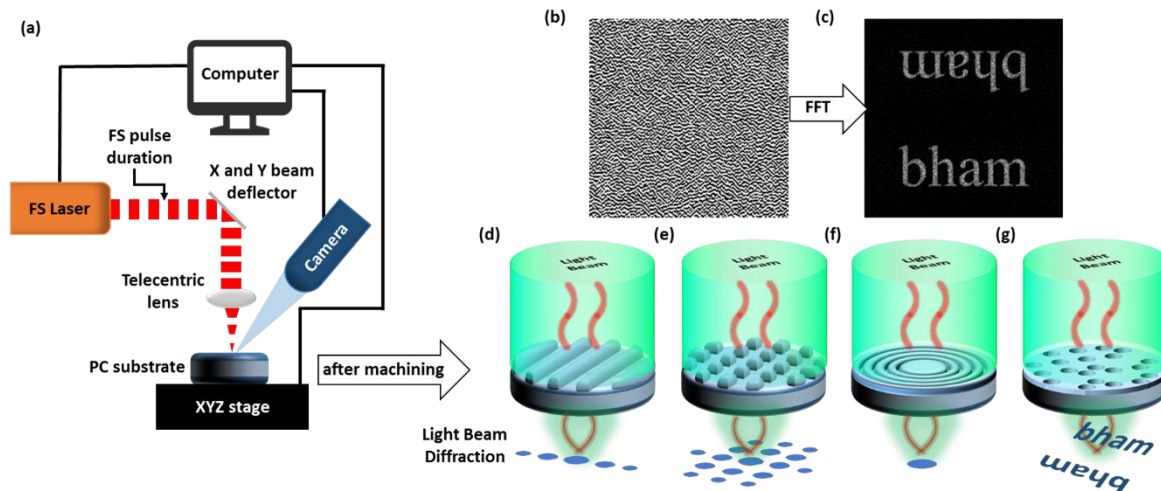
Figure 1. FS laser patterning of microphotonic devices. (a) A schematic of the FS laser microprocessing system. (b) Image of a 2D computed hologram based on 200×200 square array of aligned microgrooves. (c) A 2D Fast Fourier Transform of an image producing a light scattering pattern showing the first order of 'bham' diffraction. The zero order produced in the center of the image was reduced to view the pattern clearly. The schematics of optical devices: (d) 1D grating, (e) 2D grating, (f) FZP lens, and (g) hologram.

1/2D transmission gratings were designed to disperse incident light on the opposite side of the grating at a specific angle and direction. The dispersion of light depends on the angle of incidence and groove spacing. As the angle of incidence increases or the groove spacing decreases, the dispersion of light increases. This is based on the grating equation when light is normally incident on the microphotonic structures; in $d \sin \theta_m = n \lambda$, where d is the distance from the center of one groove to another adjacent groove, θ_m is the angle of diffraction measured from the normal, n is the order of diffraction, and λ is the diffracted wavelength[36]. For a 1D grating, the periodic grooves (d=25 µm) were designed to be parallel to each other (Figure 1d); while the periodic grooves (d=35 µm) were designed to be perpendicular to each other for the 2D grating (Figure 1e). These images show the incident light dispersion after passing through periodic grooves to produce a diffraction pattern. The profile of groove grating affects the profile of the transmitted light diffraction.

A FZP lens consists of a series of concentric annular grooves resembling rings ablated on a PC substrate (Figure 1d). This FZP lens reduces the amount of material required for its fabrication as compared to the conventional lens or blazed Fresnel lens production. The

rings diffract light to create constructive interference based on alternating transparent and opaque zones. These zones on the lens have been designed to operate in the optical regime. Therefore, to pattern the alternating zones by FS laser ablation, it is necessary to study the limitation of the spot size of the laser beam (20 µm). This led us to determine the radius (d) of rings and their numbers(n) with the wavelength of incident light (λ) to measure the focal length, $f = d^2/n\lambda,\ (n = 1,2,3\dots)$ [37], where d is the radius and n is the number of rings, and λ is the wavelength of the incident light [38-40]. The focal length and optical wavelength were set to (f=39.5 cm for 633 nm, 47 cm for 533 nm, and 56 cm for 450 nm) with nine rings. Due to fabrication on a transparent PC substrate, the lens operates in the transmission mode. The key advance in the fabrication of the lenses is their thin, lightweight construction in a variety of sizes for light gathering for use in a wide range of research and industrial applications.

A computer-generated 2D hologram consists of an array of vertically aligned microgrooves in a PC substrate. The circular pixels produce binary phase pattern which provide broad viewing angles and high-resolution image quality [41]. This microgroove array was produced by a direct FS laser ablation process. The array of circular pixels diffract light to create constructive interference based on alternating transparent and "dispersive" pixels to form a diffraction pattern [42, 43]. The pixel size dictates the resolution and beam divergence [44]. Larger pixels allow the dispersion of light at a small angle but large viewing distance [45]. Here, we used a FS laser to directly create an array of vertically aligned microgrooves as diffractive patterns to produce a high resolution image in the far field. The design of microgroove array was calculated based on Fourier optics [46], to produce a 2D 'bham' diffraction pattern. The array represented a transparent

and diffractive circular pixel mask that would create a pattern in the far field similar to a Fraunhofer hologram. The PC hologram was designed as a square array of 200×200 intensity delta spaced by a lattice constant of 40 µm and a groove diameter of 20 µm. A binary amplitude array was optimized by using the Gerchberg-Saxton algorithm [47]. Figure 1bshows the optimized solution for the microgroove array based hologram. Figure 1c illustrates the 2D Fast Fourier Transform (FFT) array of the microgroove hologram. This computational approach allowed predicting the order of 'bham' diffraction for the hologram.

To fabricate optical devices, Figure 1a shows a schematic of the multiaxis laser micromachining that was utilized. FS pulses of an ultra short ytterbium-based laser (λ=1030 nm, 310 fs) have a maximum pulse energy (10 µJ), repetition rate of 500 kHz and an average power of 5 W. The FS laser system integrates a 100 mm f-theta telecentric lens to provide a focused laser beam spot diameter of 30 µm and machining field of view of 35×35 mm. This system also integrates a high dynamic scan head that is computer controlled to produce with high speed with micro patterns. The optimized laser parameters for the micromachining of the Fresnel lens, the hologram and the gratings are provided in Table 1. Furthermore, to ensure a machining accuracy of ±10 µm, a customized software was used to minimize the dynamic effects of the beam delivery subsystem on machining results during the fabrication process [27, 48, 49]. The profile of grooves was measured by a G5 Alicona Infinite system by using a 50× objective. This magnification allow a lateral resolution of 1-2 µm to be achieved and thus to image and identify the edges of microgrooves (20 µm).

Table 1. Parameters used in FS laser patterning process of optical devices

Laser parameter	Units	Fresnel Lens	Hologram	Grating (1D)	Grating (2D)
Power	W	3.5	3.5	2.2	2.2
Repetition rate	kHz	500	125	125	125
Scanning speed	m/s	2	0.5	0.5	0.5
Pulse duration	fs	310	310	310	310
Beam diameter	μm	30	30	30	30
Hatch style	-	Horizontal	Outlines	Horizontal	Horizontal and Vertical
Hatch pitch	μm	7	-	15	15
Layers	-	1	1	1	3

Optical Characterization of Microphotonic Structures

1D and 2D Transmission Gratings. Transmission gratings were designed to disperse incident light at specific angles. Angular dispersion is a function of the angle of incidence and groove spacing. The grooves were designed either to be parallel (1D grating) or perpendicular (2D grating) to each other (Figure 2d, g). The samples were studied using an optical microscope (Alicona Infinite) with 20× magnification. During the laser ablation process, some amount of the PC evaporated from the groove zone (black) and then redeposited near the groove edges. Optical microscopy measurements revealed the surface profile of these gratings showing that the width and depth of grooves were in the range of micrometer except the depth of 1D grating grooves were 550 nm.

The laser-written gratings were characterized optically, where light transmission measurements were conducted using broadband light. These measurements were performed using a spectrophotometer (2 nm resolution), which was connected to a microscope by an optical fiber. The light transmissions of the gratings were measured, where a plane PC surface was used as a reference. Figure 2a shows the average transmission spectra of 1D and 2D gratings at a normal angle of incidence. An increase in the patterned area of the grooves reduced the light transmission because of the grooves that behaved as opaque zones. The 1D and 2D gratings had ~70% and ~60% total transmission

Similarly, the light transmission through an analyzer was utilized to test the polarization of light and its effects on the diffraction in far field [50]. Both gratings nearly preserved polarization, with less than 0.6% light transmission intensity. For angular dispersion, the angle-resolved measurements were performed at a normal angle of incidence with two laser beams (455 and 533 nm) (Figure 2c). The sample was placed on a rotary stage and a detector was located 2.0 m away from the sample to obtain far field viewing distances. The stage was rotated to measure each order individually (Figure 2 f, i). Figure 2f shows the angle of diffraction pattern measured for a 1D grating illuminated at λ=450 and 533 nm with periodic grooves (d=25 µm). Well-ordered 1D diffraction patterns were observed but lower intensity was noticed for zero order in transmission mode at λ=450 nm and zero order had a comparable light intensity with the second order. This is due to the effect of two dimensional phase modulation produced by changing the depth of grooves. Additionally, light diffraction patterns were captured using a digital camera. Figure 2b shows a schematic of the experimental setup to capture this pattern. The sample was placed on a rotation stage and a semi-transparent glass globe was positioned 55 cm away parallel to the sample surface plane. This setup is suitable for light interference measurements as it has a far reaching view of the grating diffraction. The diffraction grating captured by the digital camera was in agreement with the simulated results. The fifth order diffraction pattern, for green, and the third order diffraction pattern for blue consisted of two symmetrically conjugate spot diffractions located on the opposite sides of the semitransparent global screen. The diffraction results were consistent with Bragg's law, where the diffraction spot dispersed at a larger angle producing larger diffraction as the wavelength of the laser beam increased. The image of the 1D grating

showed well-ordered bright spots on a large scale with a longer viewing distance as compared to 1D holographic gratings [51, 52]. Using the same interrogation setup, the 2D grating was analyzed. In the 2D grating, the diffraction split into multiple spots on the horizontal and vertical planes. Figure 2g shows that the width and depth of the grooves increased when they crossed each other because laser ablation was duplicated at the cross point. This process changed the structure from a square to a squircle and the diffraction pattern showed this geometry (Figure 2h). In general, although both gratings produced less diffraction orders once the wavelength of the incident light decreased, they maintained a high diffraction order as compared to the 2D holographic gratings [51, 52].
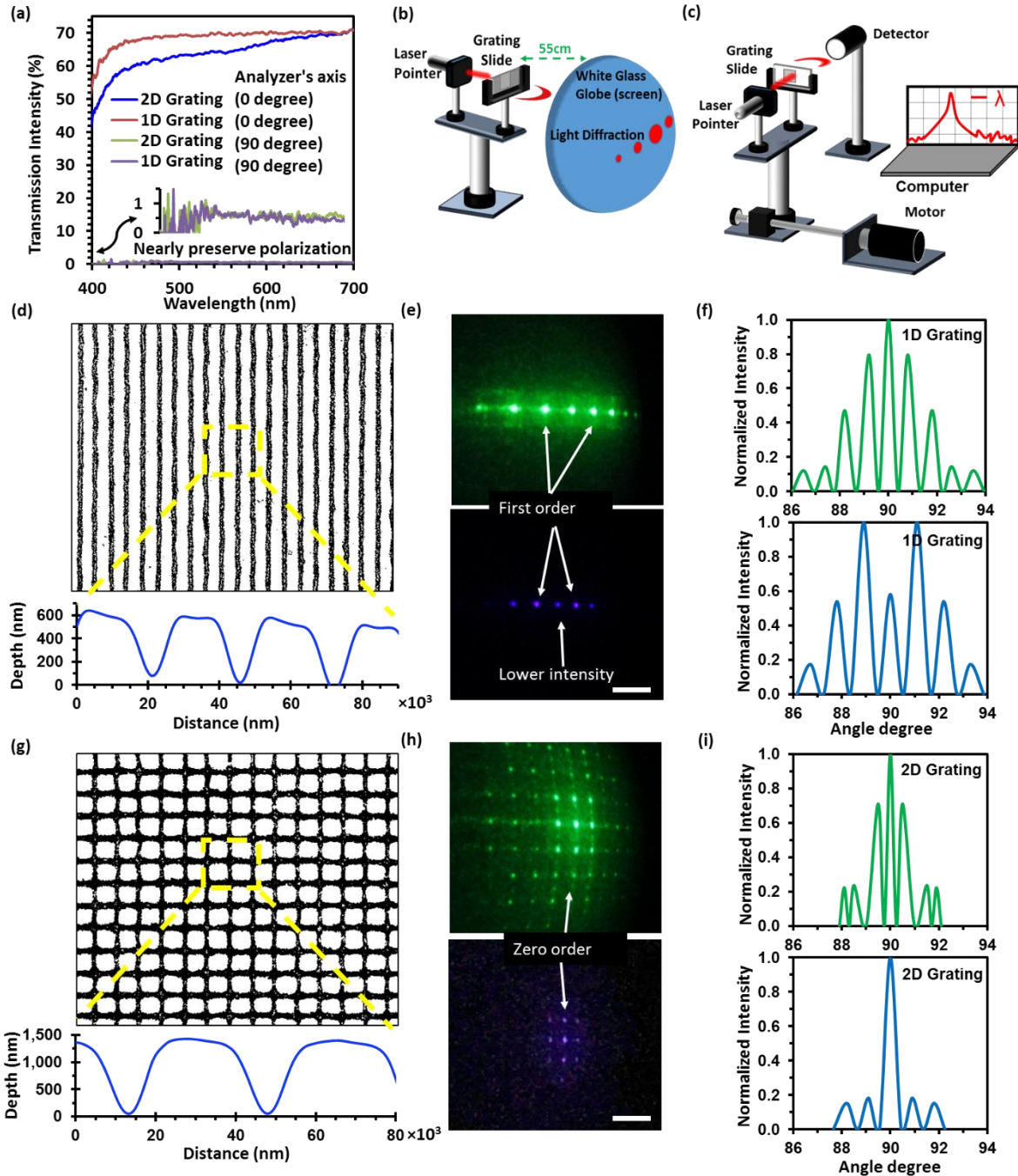
Figure 2. FS laser processing of PC 1D and 2D gratings and analyses of their optical characteristics. (a) Spectroscopic transmission measurements of the 1D and 2D gratings using broadband light at normal incidence. (b) Schematic of the experimental setup used to capture the 2D pattern from 1D and 2D gratings as seen in (e and h). (c) Schematic of

the experimental setup of angle-resolved spectral measurements in (f and i). (d- f) Spectrum analysis of the 1D grating. (g-i) Optical measurements of 2D grating. (d, g) Optical microscope images of the groove surfaces at normal incidence and their corresponding surface profiles. (e, h) 2D views of grating diffraction in a semi-transparent globe using 533 and 450 nm beams at normal incidence illumination (scale bar= 2 cm). (f, i) The angle of diffraction pattern from the grating illuminated normally at λ=450 and 533 nm.

To simulate the diffraction effect, the Geometrical Theory of Diffraction GTD was used [53]. The effect of the two-dimensional groove was modeled with a two-dimensional phase modulation in a plane. The phase modulation was produced because of the difference in the path of the light beam at different depths of the grooves. The phase difference θ at different depths of the groove $z(x,y)$ in the plane x-y is:

$$\theta(x,y) = z(x,y)k_1 + (z_{max} - z(x,y))k_0 \qquad \text{(Eq. 1)}$$

where k_1 and k_0 are the wavevectors of the PC substrate and vacuum respectively and z_{max} is the maxima. The phase difference reduces to:

$$\theta(x,y) = z(x,y)(k_1 - k_0) + \phi \qquad \text{(Eq. 2)}$$

where ϕ is an arbitrary phase constant. Thus, the modulated complex-valued 2D wave is:

$$I(x,y) = I_0(x,y) \, e^{i\,\theta(x,y)} \qquad \text{(Eq. 3)}$$

where I_0 represents the intensity profile of the laser beam (Gaussian beam illumination). Finally, the Fourier transform of $I(x,y)$ was applied to obtain the diffraction pattern observed at the far-field.

The characteristics of the groove were measured to simulate the depth profile in z(x,y). In the present case, the groove was observed with an inverted Gaussian shape. This Gaussian distribution was repeated periodically in the vertical axis, or in both, vertical and horizontal axes. The full width at half maximum utilized was 8 µm which corresponded to the size of the laser beam writing spot. The maximum height of the Gaussian distribution was selected according to the measurements. The 1D grating was simulated to have a profile depth (950 nm), refractive index (1.53), grating pitch (25.5 µm), groove width (10 µm) and analyzed at various spectrum ranges (633, 533 and 450 nm). 2D grating was simulated similarly, except profile depth (1450 nm) and grating pitch (35.2 µm) were varied. Figure 3 shows that the simulation results of the diffraction pattern observed at various wavelengths for 1D (Figure 3a) and 2D gratings (Figure 3c) and their intensity profiles of each diffraction order (b and d), respectively. Variation in the wavelength and groove depth changed the intensity profiles of each diffraction order. Furthermore, the intensity profile of each orders for 1D grating were analyzed across various groove depths (200 to 2000 nm). Controlling the depth of the groove grating allowed modulating the profile of the transmitted light diffraction.
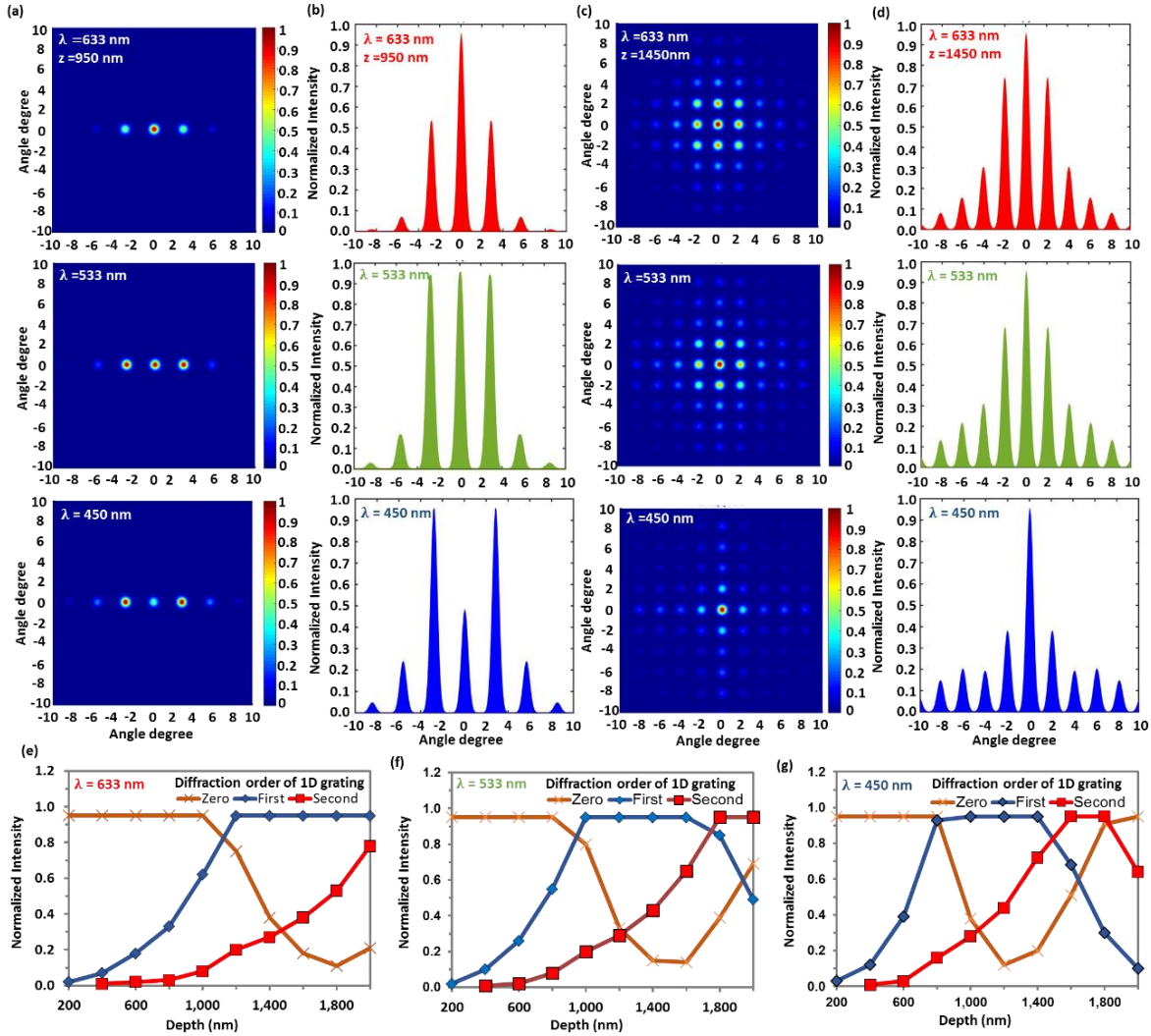
Figure 3. Simulation results of radiant intensity profile diffracted by the phase modulation from a 2D groove. (a) Diffraction pattern for 1D grating at 633 nm, 533 nm and 450 nm (top, middle and bottom panels, respectively). (b) Radiant intensity profile normal to the vertical axis for the 1D grating. (c) Diffraction pattern for a 2D grating at three different wavelengths (633, 533 and 450 nm) and their radiant intensity diffraction. (d) Radiant intensity profile normal to the vertical axis for the 2D grating. (e-g) Intensity of each diffraction orders (1D grating) across groove depth change for various incident light wavelengths (633, 533 and 450 nm).

Fresnel zone plate (FZP) lens

A FZP lens was designed to focus incident light into a bright spot at the center within a focal length range. The fabricated PC FZP lens was characterized under an optical microscope (Alicona G5 Infinite Focus) at 5× magnification to allow imaging the whole lens. Figure 4a illustrates the microscopic image of the FZP lens showing contrast between the series of concentric annular grooves (black zones) and the non-ablated PC substrate (white zones). The profile of FZP lens grooves were measured to understand the laser patterning process (Figure 4d). The laser patterning process redeposited the ablated material toward the edges, and the bottom of the grooves had a rough surface. Such rough surfaces consisting of nano- and microparticles have been reported in other materials such as buckypaper and float glass substrate [27, 54, 55]. Such artefacts in the optical device causes electron-phonon scattering, which is the main factor in the loss of energy.

The optical characteristics of the FZP lens fabricated on PC substrate were analyzed using a spectroscopy setup and an optical microscope. An optical beam profile was conducted using three different laser wavelengths (633, 533 and 450 nm) on an interrogation setup (Figure 4b). A high order diffraction from the ablated Fresnel zones showed that most of the grooves were successfully created and behaved as opaque zones. Figure 4e illustrates that incident light from a series of non-ablated zones were focused into a bright spot in the center with a focal length (f) depending on the incident wavelength (f=39 cm in 633 nm, 47 cm in 533 nm and 56 cm in 450 nm). Light focusing at focal points were observed in the long-distance far field. Figure 4f shows the 2.5D beam profile intensity of images illustrated in Figure 4e. The three different laser beams focused higher intensity spots by bending parallel light to a common focal length. Therefore, the FZP lens

works sufficiently within the visible spectrum and the light focusing effect results were in agreement with the analytical solution and simulated FFT model (Figure 4h,i). The light transmission efficiency of the FZP lens was measured as ~55% across the visible spectrum and the polarization analyzer was oriented from 0° to 90°, where a non-patterned PC substrate was the reference. This setup was used to analyze the linear polarization of light, which can affect light focusing of lens. In the present work, lenses nearly preserved the polarization (0.9%) in transmission mode (Figure 4c). Furthermore, the light transmission efficiency of the lens could be improved by increasing the contrast between the transparent and opaque zones; thus, reducing the roughness on the side and bottom of the grooves during laser ablation process can improve the lens focusing efficiency.
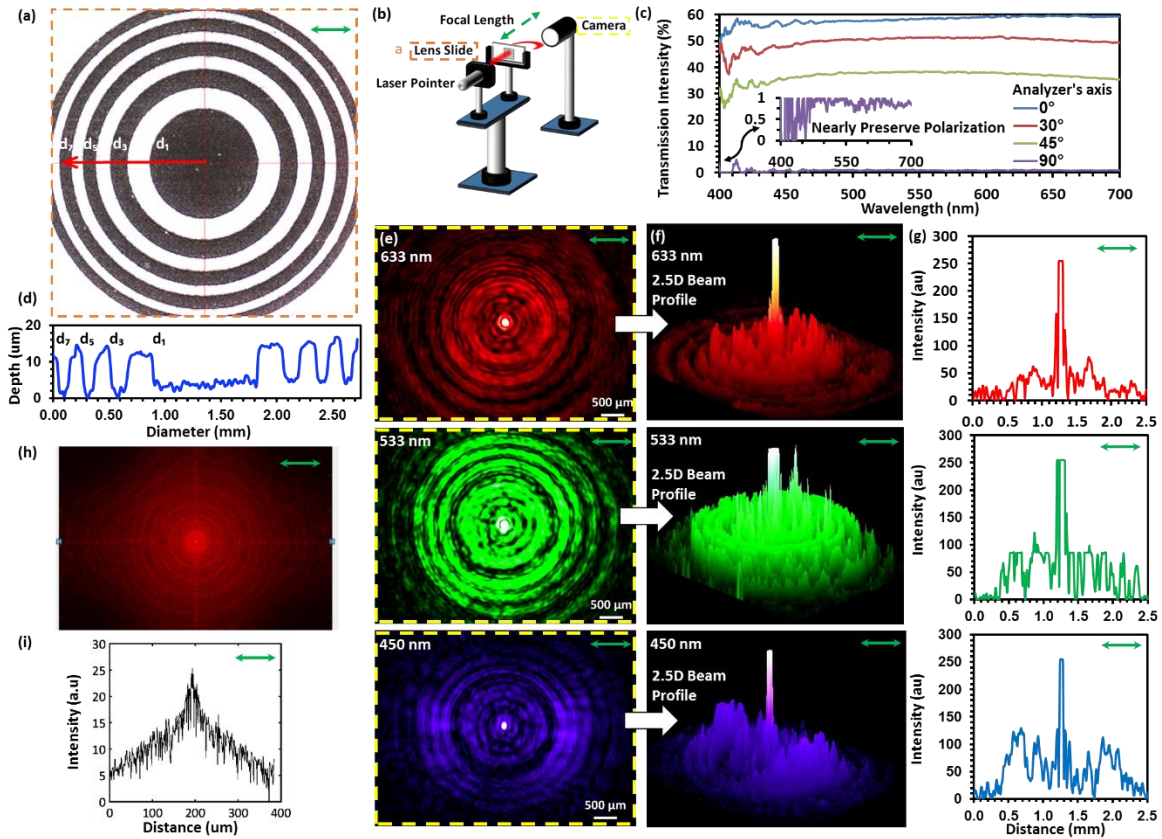
Figure 4. FS laser writing of PC FZP lenses and analyses of their surface topography and optical characteristics. (a) Optical microscope image of concentric annular grooves in the FZP lenses fabricated using FS laser ablation and corresponding groove profile in (d). (b) Schematic of experimental setup to capture the bright spot in the center of the image. (c) Transmission measurement through lens and analyzer's axis (0°, 30°, 45°, and 90°) was changed to study the polarization of light. (d) Depth profile of the grooves. (e) 633, 533 and 450 nm beams illuminated through the lens in transmission mode. The observed patterns from the lens were recorded by a high-resolution camera and their corresponding 2.5D profile images are shown in (f). (g) The intensity profile of 633, 533 and 450 nm beams at certain focal length points. (h) FFT simulated model of FZP lens and (i) its intensity profile.

Computer-generated 2D transmission hologram

A 2D array of circular pixels was designed to produce a holographic projection image. The fabricated array of vertically aligned microgrooves as circular pixels were characterized using an optical microscope at normal incidence (Figure 5b). Figure 5f shows a magnified view of the microgrooves. These microscopic images showed the contrast between the ablated circular pixels (black) and the non-ablated pixels (white). Some amount of PC evaporated from groove zones (black) and then redeposited near the groove edges during the laser ablation process. A FFT simulation was carried out using the designed pattern and displayed 'bham' diffraction symmetrically located around the center of zero order in transmission mode (Figure 5a). The highly-intense zero order of the non-diffracted light was reduced from FFT image to clarify the 'bham' diffraction. Additionally, the optical behavior of the hologram based on the microgroove array was experimentally characterized. The PC hologram was mounted onto a slide holder with a white screen located 2.5 m away to capture the diffraction pattern in the long-distance far field. The white screen was aligned parallel to the surface plane of the hologram substrate and a digital camera was placed in front of the screen. Laser beams (633, 532 and 450 nm) were normally positioned behind the hologram incident to the substrate. A transmission diffraction pattern was produced when the PC hologram was illuminated with laser beams. Figure 5c shows captured diffraction pattern images, which were consistent with the computed FFT diffraction pattern (Figure 5a). The first order diffraction pattern consisted of two symmetrically conjugate 'bham' diffraction patterns located on the opposite sides of the white screen. A clear and intense 'bham' diffraction was produced at a long viewing distance with a wide field of view. Furthermore, the wavelength dependence of the

diffraction from the PC hologram was also studied. The microscale dimensions of the 2D holographic array produced diffraction at a long viewing distance. According to Bragg's law, the diffraction angle depends on illumination wavelength. The diffraction pattern from the PC hologram was studied under red (633 nm), green (533 nm) and blue (450 nm) laser beams. The 'bham' diffraction pattern was projected at the long-distance far field producing large images as the laser wavelength increased (Figure 5c). The diffraction results were consistent with Bragg's law[56]. The images for the blue laser had low quality as the diffraction angles were close to the zero order making it hard to image the hologram. The intensity profile of "bham" diffraction and their sizes along the x-axis were measured (Figure 5d), showing that the diffraction images with the green and blue laser were reduced by 1.5 and 2.5 cm from an original size of 6.0 cm, respectively. However, the efficiency of the PC hologram can be improved by increasing the transmission contrast between the transparent pixels and dispersive pixels. Thus, reducing the evaporation and redeposition of PC from pixel edges during laser ablation processing can improve the resolution of the hologram in the long-distance far field.
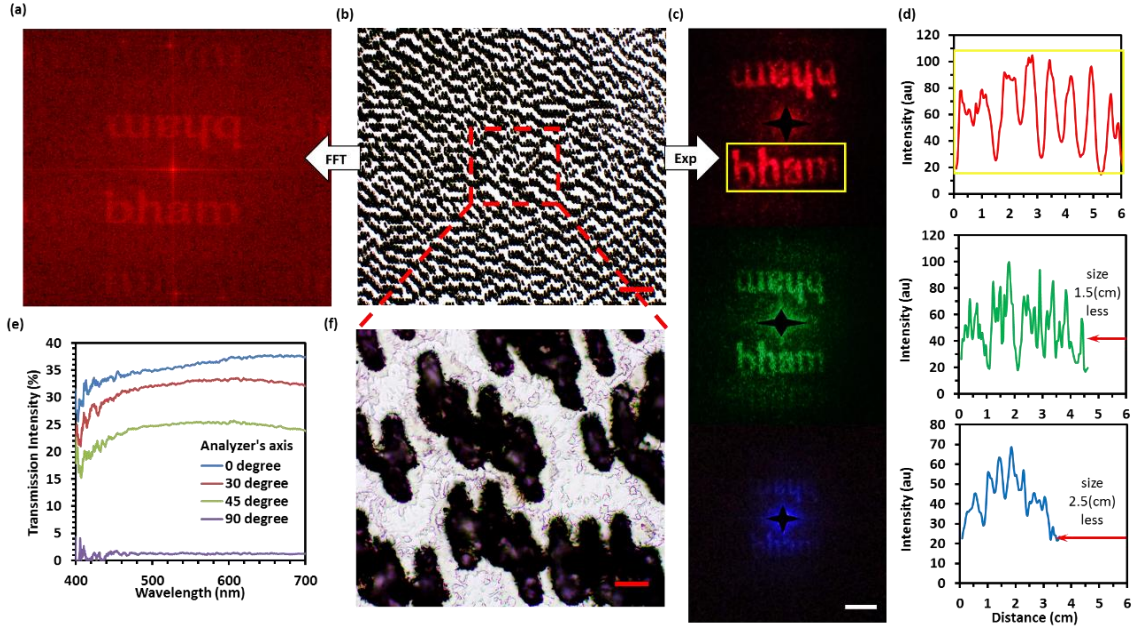
Figure 5. FS laser writing of a PC computer-generated 2D hologram. (a) Fourier transform displaying 'bham' diffraction symmetrically located around the zero order. A highly intense of zero order was excluded to clarify the first order diffraction. (b) An optical microscope image of the fabricated hologram pattern (scale bar= 200 µm). (c) The 'bham' diffraction pattern of the holographic array produced on a screen with 633, 533 and 450 nm beam illumination. Scale bar=2 cm. (d) The intensity profiles of the "bham" diffraction pattern in response to 633, 533 and 450 nm wavelength beams. (e) Light transmission intensity of the holographic pattern with different probe orientations using broadband light at normal incidence. (f) A magnified view of the holographic array. Scale bar= 20 µm.

Optical Wettability Resistance of Microphotonic Structures

Transparent devices having predefined affinity to water is highly desirable in optical and electronic devices. These hydrophilic devices may spread water across their surface to maximize contact based on the Wenzel model ($\theta < 90°$) while hydrophobic devices that naturally repel water and form droplets are defined by the Cassie-Baxter model ($90° > \theta < 150°$)[57]. The hydrophilicity of transparent devices can have a significant impact on the optical and electrical performance in a wide range of applications including self-cleaning[58, 59], anti-fouling[60], anti-corrosion[61], anti-fogging[62], icephobicity[63], and drag reduction properties[64, 65]. FS lasers can be employed not only to fabricate microphotonic devices but also modify the surface wettability resistance simultaneously, while this will require multisteps in other fabrication techniques [49].

Due to the effective wettability resistance of PC, the fabricated microphotonic devices were analyzed and tested for their surface wettability resistance. In practical applications, water contact angles (CAs) of the optical devices are measured with a deionized water droplet (5 µL) 30 days after fabrication to determine surface morphology changes over time [66]. In the present work, a water droplet from a pipette was deposited vertically along the microphotonic surface at 24 °C. A digital microscope was utilized to visualize the side profile of each deposited drop on microphotonic surfaces. The captured images were obtained after the droplet had formed its final shape to analyze the interface between the liquids and the surface of the microphotonic device. As a result, various shapes were obtained from different optical devices affecting the contact angle. Therefore, image processing was utilized to measure the contact angle of each shape. Surface wettability characterization showed that each water droplet changed their contact angle from one

device to another due to various groove depths, across groove widths and the space between them (Figure 6). PC substrate (the non-ablated area) had a contact angle of 72°, while the contact angle was reduced to 52° and 44°, achieving hydrophilicity, for 1D and 2D gratings (periodicity d=25 and 35 µm), respectively. This hydrophilic surface reduces distorted light or vision in optics during condensation by spreading water uniformly over the surface [67]. However, the contact angle for the hologram and FZP lens increased to as much as 92° and 125°, achieving hydrophobicity. Accordingly, the energy barriers associated with the local contact line depended on spacing between the microgrooves and resulted in the loss of circular symmetry in the contact line on the surface [68]. These microphotonic devices with hydrophilic and hydrophobic surfaces can be used in various optical applications such as outdoor surveillance cameras, and dynamic displays in extreme environments, biomedical optics, and endoscopy.
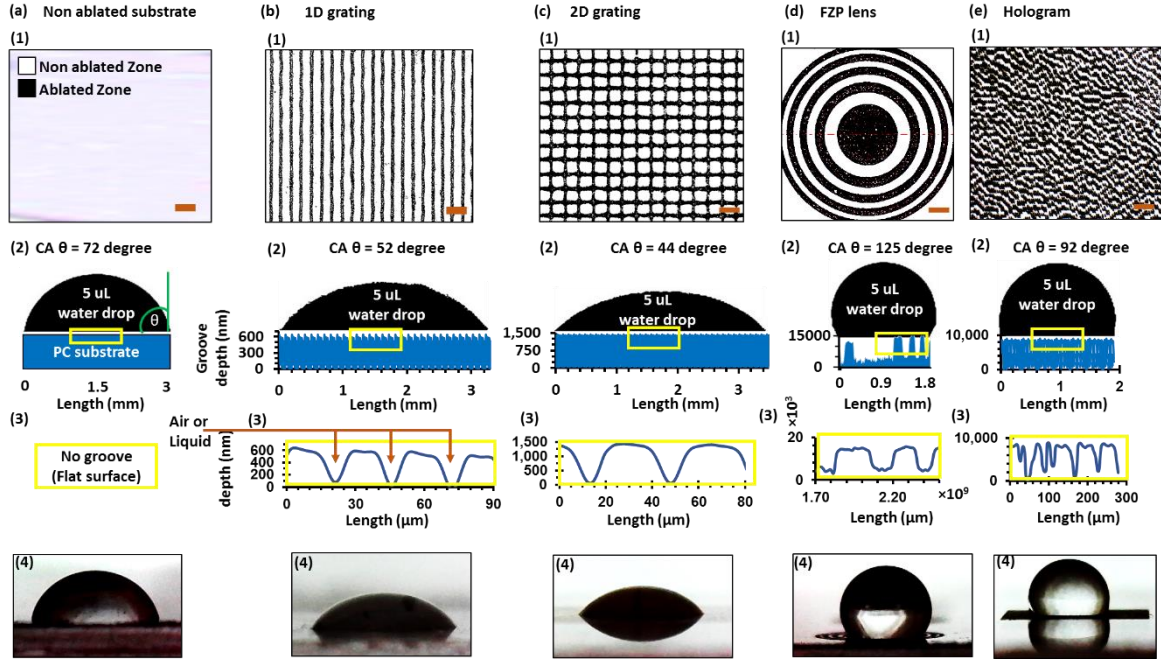
Figure 6. Water droplet contact angle for hydrophilic and hydrophobic microphotonic devices after the droplet had formed its final shape to analyze the interface between the liquids and the surfaces of the microphotonic devices. Water droplets were deposited on (a) the PC substrate with non-ablated zone, (b) 1D grating, (c) 2D grating, (d) FZP lens, and (e) hologram. Each device has been illustrated with (1) optical microscope images of the fabricated devices at normal incident, Scale bars=50, 50, 50, 400 and 400 µm respectively, (2) droplet profiles on the grooves, (3) the magnified views of groove profile, and (4) microscopic images of water droplets on optical devices.

Conclusion

The fabrication of 1D/2D gratings, a FZP lens and a 2D hologram on PC substrates was demonstrated by using direct FS laser writing. This microphotonic device fabrication approach allows creating microphotonic devices with nanoscale depth. This technique is applicable for producing 3D microphotonic devices in various polymeric and glass materials, where a few hundred nanometers in depth of 3D grooves can change the 2D phase modulation and diffraction efficiency. The major challenge in using this route for fabricating such microphotonic devices is the control and reproducibility of the 2D grooves and also minimizing the unwanted burrs on groove edges and bottom. The FS direct laser patterning technique presented in this work can enable rapid, accurate, and cost-efficient production of displays, optical filters, sensors, and fibre optic devices.

ASSOCIATED CONTENT

Supporting Information

AUTHOR INFORMATION

Corresponding Author

* talqurashi@su.edu.sa, h.butt@bham.ac.uk

Notes

We declare no competing financial interests.

References

1. Sun, Y.-L., et al., *Protein-based soft micro-optics fabricated by femtosecond laser direct writing.* Light Sci Appl, 2014. **3**: p. e129.
2. Fang, R., A. Vorobyev, and C. Guo, *Direct visualization of the complete evolution of femtosecond laser-induced surface structural dynamics of metals.* Light Sci Appl., 2017. **6**: p. e16256.
3. Zhao, Q.-Z., et al., *Direct writing computer-generated holograms on metal film by an infrared femtosecond laser.* Optics Express, 2005. **13**(6): p. 2089-2092.
4. Kerse, C., et al., *Ablation-cooled material removal with ultrafast bursts of pulses.* Nature, 2016. **537**(7618): p. 84-88.
5. Du, D., et al., *Laser-induced breakdown by impact ionization in SiO2 with pulse widths from 7 ns to 150 fs.* Applied Physics Letters, 1994. **64**(23): p. 3071-3073.
6. Pronko, P.P., et al., *Machining of sub-micron holes using a femtosecond laser at 800 nm.* Optics Communications, 1995. **114**(1): p. 106-110.
7. Joglekar , A.P., et al., *A study of the deterministic character of optical damage by femtosecond laser pulses and applications to nanomachining.* Applied Physics B, 2003. **77**(1): p. 25-30.
8. Chimmalgi, A., et al., *Femtosecond laser aperturless near-field nanomachining of metals assisted by scanning probe microscopy.* Applied Physics Letters, 2003. **82**(8): p. 1146-1148.
9. Sugioka, K. and Y. Cheng, *Ultrafast lasers[mdash]reliable tools for advanced materials processing.* Light Sci Appl, 2014. **3**: p. e149.
10. Brabec, T. and F. Krausz, *Intense few-cycle laser fields: Frontiers of nonlinear optics.* Reviews of Modern Physics, 2000. **72**(2): p. 545-591.
11. Chris, B.S., B. André, and M. Eric, *Laser-induced breakdown and damage in bulk transparent materials induced by tightly focused femtosecond laser pulses.* Measurement Science and Technology, 2001. **12**(11): p. 1784.
12. Steinmeyer, G., et al., *Frontiers in Ultrashort Pulse Generation: Pushing the Limits in Linear and Nonlinear Optics.* Science, 1999. **286**(5444): p. 1507-1512.
13. Li, Q., K. Nakkeeran, and P.K.A. Wai, *Ultrashort pulse train generation using nonlinear optical fibers with exponentially decreasing dispersion.* Journal of the Optical Society of America B, 2014. **31**(8): p. 1786-1792.
14. Kumar, K., et al., *Quantized structuring of transparent films with femtosecond laser interference.* Light Sci Appl, 2014. **3**: p. e157.
15. Wu, D., et al., *In-channel integration of designable microoptical devices using flat scaffold-supported femtosecond-laser microfabrication for coupling-free optofluidic cell counting.* Light Sci Appl, 2015. **4**: p. e228.
16. Chichkov, B.N., et al., *Femtosecond, picosecond and nanosecond laser ablation of solids.* Applied Physics A, 1996. **63**(2): p. 109-115.
17. Stuart, B.C., et al., *Nanosecond-to-femtosecond laser-induced breakdown in dielectrics.* Phys Rev B Condens Matter, 1996. **53**(4): p. 1749-1761.
18. Liu, X., D. Du, and G. Mourou, *Laser ablation and micromachining with ultrashort laser pulses.* IEEE Journal of Quantum Electronics, 1997. **33**(10): p. 1706-1716.
19. Gattass, R.R. and E. Mazur, *Femtosecond laser micromachining in transparent materials.* Nat Photon, 2008. **2**(4): p. 219-225.

20. Osellame, R., G. Cerullo, and R. Ramponi, *Femtosecond Laser Micromachining: Photonic and Microfluidic Devices in Transparent Materials*. 2012: Springer Berlin Heidelberg.

21. Li, Y., et al., *Single femtosecond pulse holography using polymethyl methacrylate.* Optics Express, 2002. **10**(21): p. 1173-1178.

22. Feng, P., et al., *Femtosecond laser-induced subwavelength ripples formed by asymmetrical grating splitting.* Applied Surface Science, 2016. **372**: p. 52-56.

23. Kawamura, K.-i., et al., *Holographic encoding of fine-pitched micrograting structures in amorphous SiO2 thin films on silicon by a single femtosecond laser pulse.* Applied Physics Letters, 2001. **78**(8): p. 1038-1040.

24. Wang, C., et al., *Anisotropic optical transmission of femtosecond laser induced periodic surface nanostructures on indium-tin-oxide films.* Applied Physics Letters, 2012. **101**(10): p. 101911.

25. Matsuo, S., S. Juodkazis, and H. Misawa, *Femtosecond laser microfabrication of periodic structures using a microlens array.* Applied Physics A, 2005. **80**(4): p. 683-685.

26. Bricchi, E., et al., *Birefringent Fresnel zone plates in silica fabricated by femtosecond laser machining.* Optics Letters, 2002. **27**(24): p. 2200-2202.

27. Deng, S., et al., *Laser directed writing of flat lenses on buckypaper.* Nanoscale, 2015. **7**(29): p. 12405-12410.

28. Valle, G.D., R. Osellame, and P. Laporta, *Micromachining of photonic devices by femtosecond laser pulses.* Journal of Optics A: Pure and Applied Optics, 2009. **11**(1): p. 013001.

29. Scardaci, V., et al., *Carbon Nanotube Polycarbonate Composites for Ultrafast Lasers.* Advanced Materials, 2008. **20**(21): p. 4040-4043.

30. Aden, M., A. Roesner, and A. Olowinsky, *Optical characterization of polycarbonate: Influence of additives on optical properties.* Journal of Polymer Science Part B: Polymer Physics, 2010. **48**(4): p. 451-455.

31. Zhu, Y., C. Romain, and C.K. Williams, *Sustainable polymers from renewable resources.* Nature, 2016. **540**(7633): p. 354-362.

32. Chen, J.-g., et al., *Low-loss planar optical waveguides fabricated from polycarbonate.* Polymer Engineering & Science, 2009. **49**(10): p. 2015-2019.

33. Takahiro, I., M. Tetsuya, and U. Tatsuo, *Wide-Viewing-Angle Polarizer with a Large Wavelength Range.* Japanese Journal of Applied Physics, 2002. **41**(7R): p. 4553.

34. Ueda, M., *A study on the characteristics of antiplasticized polycarbonates and their optical disk substrates.* Polymer Engineering & Science, 2004. **44**(10): p. 1877-1884.

35. Butt, H., et al., *Carbon Nanotube Based High Resolution Holograms.* Advanced Materials, 2012. **24**(44): p. OP331-OP336.

36. Deng, S., et al., *Graphene nanoribbon based plasmonic Fresnel zone plate lenses.* RSC Advances, 2017. **7**(27): p. 16594-16601.

37. Di Fabrizio, E., et al., *High-efficiency multilevel zone plates for keV X-rays.* Nature, 1999. **401**(6756): p. 895-898.

38. Rajasekharan, R., et al., *Can nanotubes make a lens array?* Adv Mater, 2012. **24**(23): p. Op170-3.

39. Deng, S., et al., *Computational modelling of a graphene Fresnel lens on different substrates.* RSC Advances, 2014. **4**(57): p. 30050-30058.

40. Kong, X.-T., et al., *Graphene-Based Ultrathin Flat Lenses.* ACS Photonics, 2015. **2**(2): p. 200-207.

41. Ma, X., et al., *Analysis of optical characteristics of modulation devices with square and circle pixels for 3D holographic display.* Chinese Optics Letters, 2015. **13**(1): p. 010901-010901.

42. Larouche, S., et al., *Infrared metamaterial phase holograms.* Nat Mater, 2012. **11**(5): p. 450-454.

43. Montelongo, Y., et al., *Computer generated holograms for carbon nanotube arrays.* Nanoscale, 2013. **5**(10): p. 4217-4222.

44. Wakunami, K., et al., *Projection-type see-through holographic three-dimensional display.* Nature Communications, 2016. **7**: p. 12954.

45. Hainich, R.R. and O. Bimber, *Displays: Fundamentals & Applications, Second Edition*. 2016: CRC Press.

46. Goodman, J.W., *Introduction to Fourier Optics*. 2005: W. H. Freeman.

47. Gerchberg, R.W. and W.O. Saxton, *A practical algorithm for the determination of the phase from image and diffraction plane pictures.* Optik (Jena), 1972. **35**: p. 237.

48. Bhaduri, D., et al., *An investigation of accuracy, repeatability and reproducibility of laser micromachining systems.* Measurement, 2016. **88**: p. 248-261.

49. Penchev, P., et al., *Generic software tool for counteracting the dynamics effects of optical beam delivery systems.* Proceedings of the Institution of Mechanical Engineers, Part B: Journal of Engineering Manufacture, 2017. **231**(1): p. 48-64.

50. Ingersoll, L.R., *Polarization of Radiation by Gratings.* Polarization of Radiation by Gratings, 1920. **51**: p. 129.

51. Ahmed, R., et al., *Printable ink lenses, diffusers, and 2D gratings.* Nanoscale, 2017. **9**(1): p. 266-276.

52. AlQattan, B., et al., *Holographic direct pulsed laser writing of two-dimensional nanostructures.* RSC Advances, 2016. **6**(112): p. 111269-111275.

53. Zhou, G., et al., *Superhydrophobic self-cleaning antireflective coatings on Fresnel lenses by integrating hydrophilic solid and hydrophobic hollow silica nanoparticles.* RSC Advances, 2013. **3**(44): p. 21789-21796.

54. Xue, C.-H., X. Bai, and S.-T. Jia, *Robust, Self-Healing Superhydrophobic Fabrics Prepared by One-Step Coating of PDMS and Octadecylamine.* Scientific Reports, 2016. **6**: p. 27262.

55. Alqurashi, T., et al., *Femtosecond laser directed fabrication of optical diffusers.* RSC Advances, 2017. **7**(29): p. 18019-18023.

56. Butt, H., et al., *Devitrite-Based Optical Diffusers.* ACS Nano, 2014. **8**(3): p. 2929-2935.

57. Wang, G., et al., *Robust superhydrophobic surface on Al substrate with durability, corrosion resistance and ice-phobicity.* Scientific Reports, 2016. **6**: p. 20933.

58. Alqurashi, T., et al., *Nanosecond pulsed laser texturing of optical diffusers.* AIP Advances, 2017. **7**(2): p. 025313.

59. Gauthier, A., et al., *Water impacting on superhydrophobic macrotextures.* Nature Communications, 2015. **6**: p. 8001.

60. Zhou, H., et al., *Fluoroalkyl Silane Modified Silicone Rubber/Nanoparticle Composite: A Super Durable, Robust Superhydrophobic Fabric Coating.* Advanced Materials, 2012. **24**(18): p. 2409-2412.

61. Lee, C. and C.-J. Kim, *Underwater Restoration and Retention of Gases on Superhydrophobic Surfaces for Drag Reduction.* Physical Review Letters, 2011. **106**(1): p. 014502.

62. Lu, Y., et al., *Robust self-cleaning surfaces that function when exposed to either air or oil.* Science, 2015. **347**(6226): p. 1132-1135.

63.   Wu, G., et al., *A Versatile Approach towards Multifunctional Robust Microcapsules with Tunable, Restorable, and Solvent-Proof Superhydrophobicity for Self-Healing and Self-Cleaning Coatings.* Advanced Functional Materials, 2014. **24**(43): p. 6751-6761.

64.   Keller, J.B., *Geometrical Theory of Diffraction*.* Journal of the Optical Society of America, 1962. **52**(2): p. 116-130.

65.   Wisdom, K.M., et al., *Self-cleaning of superhydrophobic surfaces by self-propelled jumping condensate.* Proceedings of the National Academy of Sciences, 2013. **110**(20): p. 7992-7997.

66.   Liu, Y., et al., *Pancake bouncing on superhydrophobic surfaces.* Nat Phys, 2014. **10**(7): p. 515-519.

67.   Yu, E., et al., *Extreme wettability of nanostructured glass fabricated by non-lithographic, anisotropic etching.* Scientific Reports, 2015. **5**: p. 9362.

68.   Raj, R., et al., *High-resolution liquid patterns via three-dimensional droplet shape control.* Nature Communications, 2014. **5**: p. 4975.